PAPER • OPEN ACCESS

Effect of blade contamination on power production of wind turbines

To cite this article: Serkan Özgen *et al* 2022 *J. Phys.: Conf. Ser.* **2265** 032012

View the article online for updates and enhancements.

Effect of blade contamination on power production of wind turbines

Serkan Özgen[1], Eda Bahar Sarıbel[2], Ali Rıza Yaman[3]

[1]Middle East Technical University, Dept. Aerospace Eng., 06800, Ankara, Turkey
[2]AEROMS Engineering, Inc., Middle East Technical University Technopolis, 06800, Ankara, Turkey
[3]Borusan EnBW, 33600, Mersin, Turkey

E-mail: `serkan.ozgen@ae.metu.edu.tr`

Abstract. Wind turbines suffer from considerable power losses because of contamination on their blades, that can be due to erosion, wear, smog, insect, sand and dust particle impact. Blade contamination, its effects on the flows over the wind turbine blades and consequent power production losses form the main focus of the present study. These effects are mainly due to increased roughness on the blades leading to earlier laminar-turbulent transition and consequently, thicker boundary-layers on the blades. Early laminar-turbulent transition leads to a larger part of the flow over a blade being turbulent, thus increasing skin friction drag. Thicker boundary-layer on a blade results in blade profile being effectively modified, rendering the flow over the blade depart from ideal. In the present study, the effects of blade contamination on power output of contaminated wind turbine blades is investigated numerically using an in-house computational tool. Blade Element Momentum Method (BEM) combined with the Panel Method is used to calculate the local velocity and angle of attack at the blade sections, together with the power produced by the blade. Trajectories of particles causing contamination are calculated using Lagrangian approach, also yielding the impingement pattern of the particles on the blade surface, i.e. particle collection efficiency distribution. The effects of roughness on the boundary-layer flow are investigated by using an Integral Boundary-Layer Method, which yields the characteristics of the boundary-layer, i.e. laminar-turbulent transition location, increased skin-friction and thickening of the boundary-layer. The blade shape is modified due contamination thickness, the local height of which is assumed to be proportional to the local collection efficiency. Also, the roughness height distribution used in the boundary-layer calculations is assumed to be equal to the contamination thickness distribution on the blades. Power production and consequent losses of wind turbines with contaminated wind turbine blades are studied with respect to variations in particle size, wind speed and roughness height.

1. Introduction and Objectives

The efficiency of wind turbines in field operations is significantly reduced by roughness caused by contamination of their blades and erosion due to insect impact, rain contaminants, wear, smog, sand, salt and dust particles. This is mainly due to increased roughness on the blades leading to earlier laminar-turbulent transition, hence thicker boundary-layers on the blades. Depending on the severity of the conditions, up to 53% reduction in lift coefficient and 314 % increase in drag coefficient of the blade sections have been reported. It is also reported that annual energy production (AEP) due to contamination and erosion can be reduced by 2-3.7 % [1]. Although recent improvements in airfoil design and advent of pitch-controlled wind-turbines have reduced losses

due to roughness, there is still need for further improvement [2]. Computational Fluid Dynamics methods and tools can be used in order to compute the characteristics of the boundary-layer flows under roughness effects, early laminar-turbulent transition of the boundary-layer flow and consequently the effects that these have on the power production of wind turbine blades.

The problems of aircraft icing and blade contamination have similarities. Computation of both the icing and blade contamination problems involves the solution of particle trajectories and their impingement patterns on a surface. Moreover, the sizes of cloud particles and particles leading to contamination in blades have the same order of magnitude. For these reasons, existing in-flight icing prediction tools can be adapted for studying blade contamination. The in-house developed `aeromsice_bem.f` is such a tool that was first developed for ice accretion simulations on multi-element airfoils [3], later extended for ice-accretion simulations on finite wings [4], aero-engine air intakes [5] and for wind turbine blades [6]. Recently, it has been adapted for computation of blade contamination effects on wind turbine blades. The code can handle particle sizes ranging from 10 to 10000 microns, covering the range of typical contaminants in the atmosphere like very fine sand, coarse sand, fruit fly and housefly. The code determines the power output for clean and contaminated wind turbines by using blade geometry, meteorological conditions, flow conditions and contaminant size information.

The present paper aims to:

- Model surface roughness on wind turbine blades due to contamination and the consequent effects on the flow around the blade sections. Transition prediction and development of the boundary-layer are the main points of focus.
- Calculate the distribution of the roughness elements by calculating particle trajectories and consequent impingement patterns.
- Calculate power production losses of wind turbines due to blade contamination compared to clean blade power production.

2. Formulation and Methodology
The current method for the estimation of power production losses consists of three modules:

- A flow field solution module that comprises the Hess-Smith Panel Method and Blade Element Momentum Method (BEM). This module also calculates the power production of clean and contaminated wind turbine blades.
- A module that calculates the particle trajectories and the impingement patterns of the contaminants yielding the particle collection efficiency distribution.
- A module for boundary-layer flow solution using the Integral Boundary-Layer Method. In this module, the roughness distribution is used to estimate the boundary-layer parameters like the skin friction coefficient and boundary-layer displacement thickness distributions.

2.1. Flow Field Solution
2.1.1. Blade Element Momentum Method (BEM)   The geometry used in this study is the NREL 5MW turbine. A number of blade sections (elements) are selected from the 3D blade geometry for the analysis. Sections of blade are mostly chosen at 30-80% of the blade radius measured from the root of the blade, where majority of the power is produced as shown in Figure 1. Geometric propertes of the blade sections used in the computations are given in Table 1.

Blade Element Momentum Method computes the local angle of attack (α) and relative wind speed (U_{rel}), i.e. resultant velocity due to rotation and wind [7]. These parameters are calculated

using the wind speed (U), the axial and tangential induction factors (a and a'), the blade radius (R), the blade section radial position (r), the rotor rpm (Ω), rotor solidity (σ) and the blade twist (θ). The relative wind and the angle of attack at each blade element is calculated from [7]:

$$U_{rel} = \frac{U(1-a)}{sin\varphi} \tag{1}$$

$$\alpha = \varphi - \theta_i \tag{2}$$

where φ is the angle of relative wind:

$$tan\varphi = \frac{U(1-a)}{\Omega r(1+a')} \tag{3}$$

and θ_i is the twist angle of section i. The axial and tangential induction factors are given as:

$$a = \frac{1}{1 + 4F\frac{\sin^2\varphi}{\sigma c_l cos\varphi}} \tag{4}$$

$$a' = \frac{1}{\frac{4F cos\varphi}{\sigma c_l} - 1} \tag{5}$$

The lift coefficient is given by:

$$c_l = 4F sin\varphi \frac{(cos\varphi - \lambda_r sin\varphi)}{\sigma(sin\varphi + \lambda_r cos\varphi)} \tag{6}$$

The speed ratio λ_r is defined as:

$$\lambda_r = \frac{\Omega r}{U} \tag{7}$$

The power produced by each blade element is calculated from:

$$dP = \Omega dQ \tag{8}$$

where the torque is given by:

$$dQ = F\sigma\pi\rho\frac{U^2(1-a)^2}{sin^2\varphi}(c_l sin\varphi - c_d cos\varphi)r^2 dr \tag{9}$$

In the above equations, F is the tip loss factor given as:

$$F = \left(\frac{2}{\pi}\right)cos^{-1}\left[e^{-\frac{(B/2)(1-r/R)}{(r/R)sin\varphi}}\right] \tag{10}$$

In equation 8, c_l and c_d are the lift and drag coefficients of the blade section. In order to calculate the power production of the turbine, Equation 8 is integrated over the radius of the blade and then the integral is multiplied by the number of blades, B.
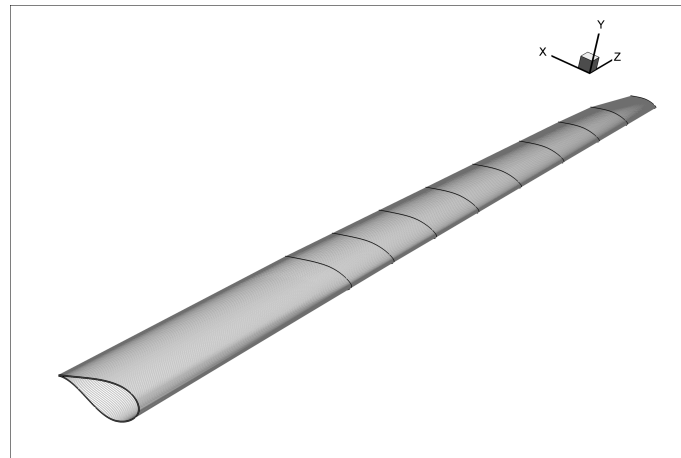
Figure 1: Blade sections of the NREL 5MW turbine used in the computations.

Table 1: Blade section characteristics of the NREL 5MW turbine used in the computations [8].

Section number	Radial position (m)	Chord length (m)	Twist angle (deg)	Airfoil
1	13.25	4.557	13.308	DU40
2	33.75	3.748	6.544	DU25
3	37.85	3.502	5.361	DU21
4	41.95	3.256	4.188	DU21
5	46.05	3.010	3.125	NACA64618
6	50.15	2.764	2.319	NACA64618
7	54.25	2.518	1.526	NACA64618
8	57.66	2.313	0.863	NACA64618
9	60.40	2.086	0.370	NACA64618
10	63.13	1.419	0.106	NACA64618

The local angle of attack and the relative wind speed are obtained using an iterative method described in [7], where convergence is achieved when the lift coefficient values computed by Equation 6 and the Panel Method become equal. The local angle of attack and the relative wind speed are then provided to the Panel Method for the computation of the flow field. The current study is conducted using 10 blade sections, where each section is represented by 201 data points.

2.1.2. Panel Method In the Panel Method, the geometry is divided into quadrilateral panels each associated with a source singularity element together with a vortex singularity that is constant for all panels. The developed computer program uses N quadrilateral panels to solve $N + 1$ singularity strengths using the flow tangency boundary condition at the collocation points of the panels and an additional equation using the Kutta condition. Once the singularity strengths are calculated, a velocity potential can be constructed and the flow velocity components at any location in the flow field can be calculated, including the boundaries of the geometry. The velocity components at a point are the x- and y-derivatives of the velocity potential constructed at that point [9]. The velocity distribution on the blade section is fed as an input the boundary-layer calculations. Off-body velocity components are used to calculate the particle trajectories.

2.2. Particle Trajectories and Collection Efficiency Calculation
This module is used to determine particle trajectories and their impingement patterns on the blade surface. This module also determines the roughness thickness distribution of the contaminants. Particle trajectory calculations are based on the Lagrangian approach assuming spherical particles, one-way interaction between particles and the flow field (presence of particles do not effect the flow-field) and aerodynamic drag and gravity being the only forces acting on the particles. The equations of motion that follow are integrated in time using an appropriate drag coefficient law that gives the particle drag force coefficient as a function of the particle Reynolds number [3]:

$$m\ddot{x}_p = -D\cos\gamma \tag{11}$$

$$m\ddot{y}_p = -D\sin\gamma - mg \tag{12}$$

$$\gamma = \tan^{-1}\frac{\dot{y}_p - V_y}{\dot{x}_p - V_x} \tag{13}$$

$$D = {}^1\!/_2\rho V_{rel}^2 C_D A_p \tag{14}$$

$$V_{rel} = \sqrt{(\dot{x}_p - V_x)^2 + (\dot{y}_p - V_y)^2} \tag{15}$$

In the above expressions, C_D is the particle drag coefficient, V_x and V_y are the components of the flow field velocity at the particle location and $\dot{x}_p$, $\dot{y}_p$, $\ddot{x}_p$, $\ddot{y}_p$ are the components of the particle velocity and acceleration. Atmospheric density and particle cross-sectional area are denoted by ρ and A_p. Drag coefficients of the particles are calculated as follows [10]:

$$C_D = \frac{24}{Re}(1 + 0.197Re^{0.63} + 2.6\times10^{-4}Re^{1.38}), Re \le 3500 \tag{16}$$

$$C_D = \frac{24}{Re}(1.699\times10^{-5})Re^{1.92}, Re > 3500 \tag{17}$$

where, $Re = \rho V_{rel}d_p/\mu$ is the Reynolds number based on particle diameter d_p, and relative velocity V_{rel}, while μ is the atmospheric viscosity. Trajectory calculations start from a sufficiently far distance from the blade leading edge (~ 10 chord lengths). The calculations for a single blade section continue until either the particle impinges on the surface or moves past the blade trailing edge. Calculations are done for a large number of particles in order to obtain an impingement distribution with sufficient resolution and accuracy on the surface. The particle trajectories calculated along the blade span for a wind speed of $U = 10$ m/s and particle diameter of $d_p = 40$ microns is illutrated in Figure 2. Notice that no particles impinge on the first section at $r = 13.25$ m becuase the particles follow the streamlines and they are deviated away from the geometry, which has the largest chord and leading edge radius for this blade section. Refer also to the discussion for Figure 3.

Differences in trajectory patterns for different particle diameters are illustrated in Figure 3 for particle diameters of $d_p = 40$ and 150 microns obtained at $r = 46.05$ m, roughly at 75% of blade radius and at a wind speed of $U = 10$ m/s. The trajectories of particles in Figure 3a follow streamlines closely, while the paricles in Figure 3b follow ballistic trajectories. Larger particles follow more ballistic trajectories due their higher mass and inertia and as a result of this, higher number of particles impinge on the surface over a wider region. This results in higher values of the collection efficiency distributed over a wider impingement zone [3]. This determines the distribution of the contaminants and their heights on the surface, as expalined below. It is known that for particles $d_p > 150$ microns, the trajectories do not vary significantly so larger particles are not included in the current study.

2.3. Boundary-Layer Solution

The current study employs an Integral Boundary-Layer Method for the calculation of the boundary-layer parameters. With this method, the details of the laminar and turbulent boundary-layers are calculated fairly accurately. Of particular interest are the skin friction coefficient and the boundary-layer displacement thickness distributions. The displacement thickness is the distance by which the external potential field of flow is displaced outwards as a consequence of the decrease in velocity in the boundary-layer [11]. In the current method, the calculated boundary-layer displacement thickness distribution is added to the original blade section geometry in order to include the effects of the viscous flow on the potential flow around the blade section. The power production is calculated using this effective geometry.
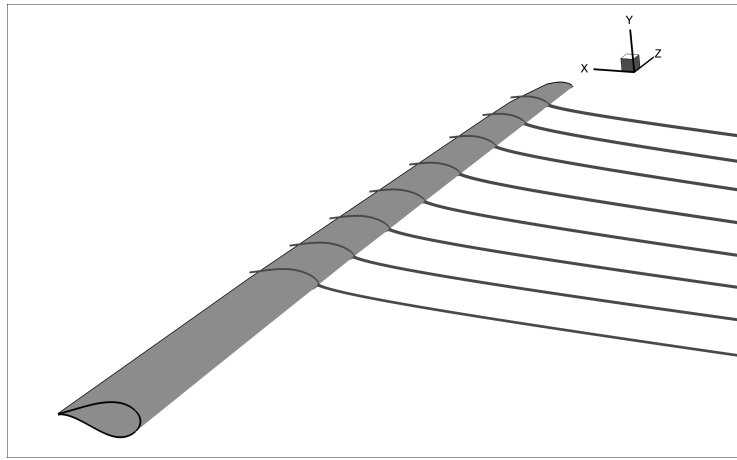

Figure 2: Particle trajectories along the span of the turbine blade ($U = 10$ m/s, $d_p = 40\mu$m.)
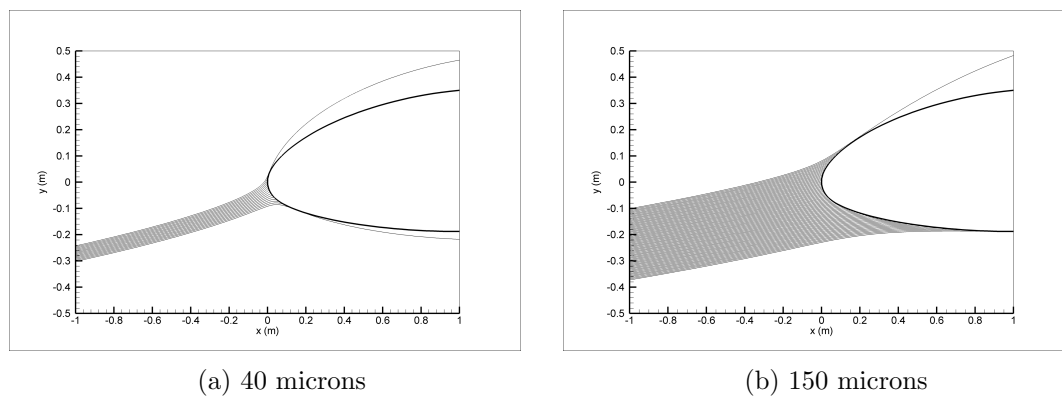

(a) 40 microns

(b) 150 microns

Figure 3: Particle trajectories for 40 microns and 150 microns ($U = 10$ m/s, $r = 46.05$ m).

The boundary-layer calculations start at the leading edge and proceed downstream using the marching technique for the upper and lower surfaces of the airfoil. Transition prediction is based on the roughness Reynolds number, $Re_k = \rho U_k k_s/\mu$ and transition is assumed to occur at $Re_k = 600$ [10], where k_s is the roughness height and U_k is the local airflow velocity at the roughness height location, calculated from the following expression [3]:

$$\frac{U_k}{U_e} = 2\frac{k_s}{\delta} - 2\left(\frac{k_s}{\delta}\right)^3 + \left(\frac{k_s}{\delta}\right)^4 + \frac{1}{6}\frac{\delta^2}{\nu}\frac{dU_e}{ds}\frac{k_s}{\delta}\left(1 - \frac{k_s}{\delta}\right)^3 \tag{18}$$

In the expression, U_e is the flow velocity outside the boundary-layer at the roughness location and s is the streamwise distance along the airfoil surface starting at the stagnation point.

The roughness height is calculated as follows:

(i) The maximum roughness height, $k_{s,max}$ is selected for the overall blade, e.g. 1mm.

(ii) This value of the roughness height is assigned to the location where the local collection efficiency is the maximum, β_{max}. This location is usually at a point on the blade section closest to the tip. There are two reasons for this, first being the blade section at the tip is usually the thinnest and the one with the shortest chord. It is known that, size reduction increases the collection efficiency [3]. Second, the total flow velocity (resultant of rotational and wind velocities) is the highest at the blade tip, increasing the collection efficiency [3].

(iii) All other points on the blade are assigned roughness heights by scaling the value selected in step i with the local collection efficiency values of individual points, β and the maximum collection efficiency value, β_{max}:

$$k_s = k_{s,max} \frac{\beta}{\beta_{max}} \tag{19}$$

The scaling approach for determining the contaminant and roughness distribution is explained graphically in Figure 4. The roughness height distribution obtained for two different particle sizes using the method outlined is illustrated in Figure 5. As can be seen, for larger particles, the collection efficiency values are higher and the impingement zone is wider, resulting in a wider contaminated zone with contamination thicknesses being higher over the overall blade. The modification of the geometry due to contamination is shown in Figure 6 for the same two particles sizes at two different radial positions, $r = 56.05$ m (75% blade radius) and $r = 63.13$ m (blade tip). As explained above, the contamination layer is thicker at the blade tip and it is spread over a wider region for the larger contaminant particles.

2.3.1. Laminar Boundary-Layer The laminar boundary layer thickness is given by [12]:

$$\delta_l = \frac{315}{37}\theta_l \tag{20}$$

The laminar boundary-layer momentum thickness is computed using Thwaites formulation [11]:

$$\frac{\theta_l^2}{\nu} = \frac{0.45}{U_e^6} \int_0^s U_e^5 ds \tag{21}$$

Boundary-layer displacement thickness is calculated from $\delta_l^* = H\theta_l$ and the boundary-layer shape factor H is calculated from [11]:

$$H = 2 + 4.14z - 83.5z^2 + 854z^3 - 3337z^4 + 4576z^5 \tag{22}$$

where $z = 0.25 - \lambda$ and $\lambda = \frac{\theta_l^2}{\nu}\frac{dU_e}{ds}$. Finally, The skin friction coefficient is calculated from [12]:

$$\frac{C_f}{2} = 0.225 \frac{\nu}{\theta_l U_e} \tag{23}$$

2.3.2. Turbulent Boundary-Layer For turbulent flow, the skin friction is calculated from the following relation [10]:

$$\frac{C_f}{2} = \frac{0.1681}{[ln(864\theta_t/k_s + 2.568)]^2} \tag{24}$$

The turbulent boundary-layer momentum thickness is computed from:

$$\theta_t = \frac{0.036\nu^{0.2}}{U_e^{3.29}} \left(\int_{s_{tr}}^{s} U_e^{3.86} ds \right)^{0.8} + \theta_{tr} \tag{25}$$

where θ_{tr} is the laminar momentum thickness at transition location. Finally, the boundary-layer displacement thickness is given by $\delta_t^* = H\theta_t$ where $H = 1.29$ [13].

The skin-friction coefficient distribution is integrated over the blade section in order to calculate the section drag coefficient, c_d. Due to contamination on the blade, the surface roughness increases, leading to earlier laminar-turbulent transition, thicker boundary-layer and higher skin friction coefficient levels. This leads to reduction in lift, incrase in drag and consequently, reduction in turbine power production.
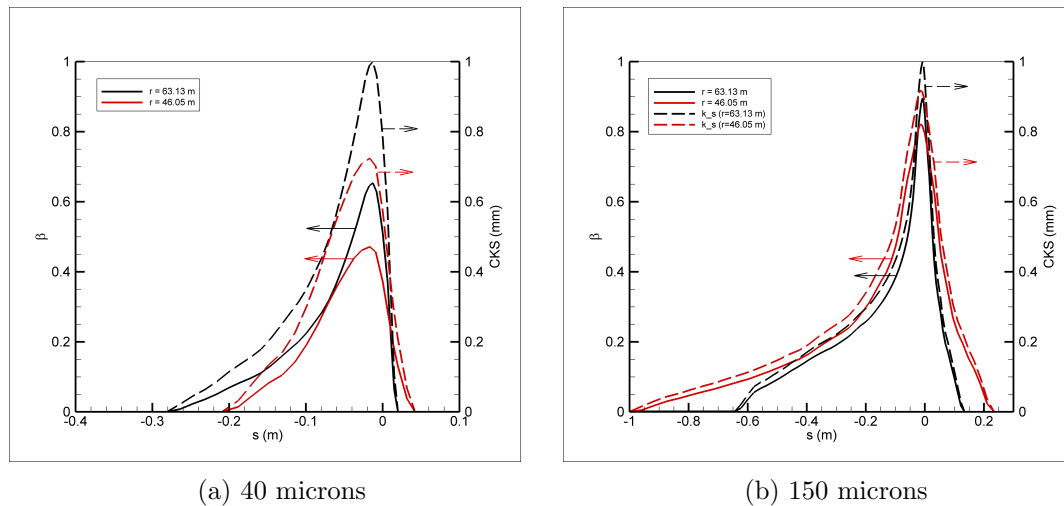

(a) 40 microns   (b) 150 microns

Figure 4: Scaling of contaminant thickness distribution with collection efficiency ($U = 10$ m/s).

(a) 40 microns   (b) 150 microns
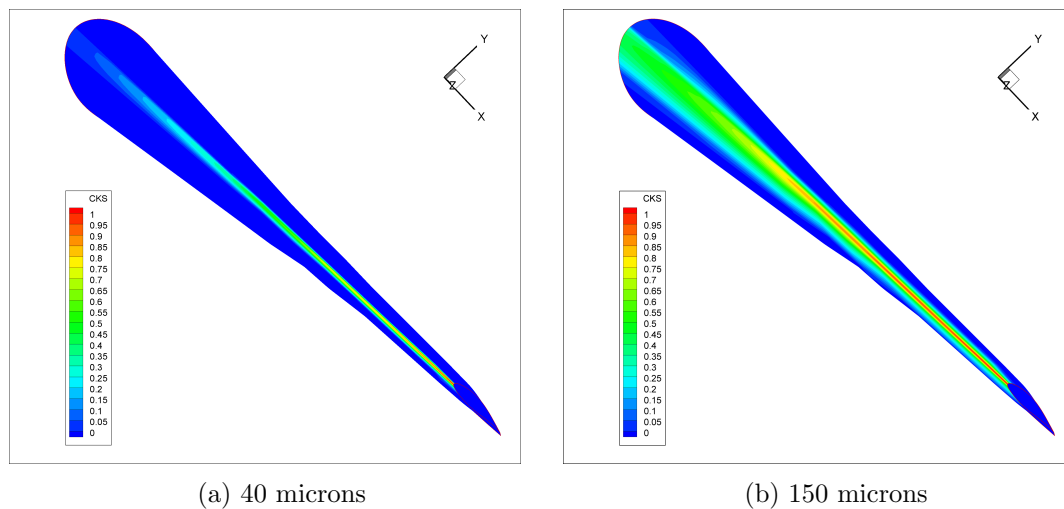
Figure 5: Contaminant thickness distribution for 40 and 150 micron particles ($U = 10$ m/s).
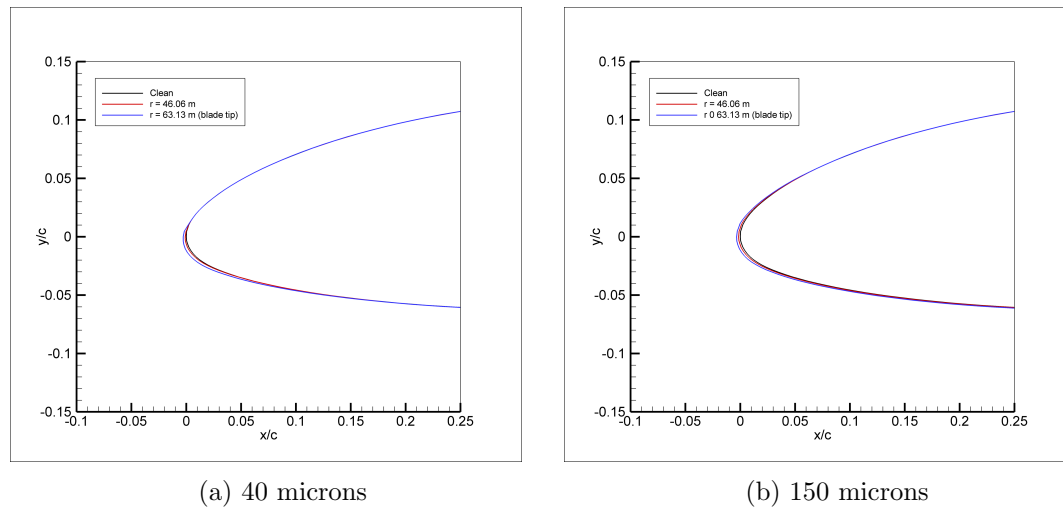
(a) 40 microns

(b) 150 microns

Figure 6: Contaminated blade sections at $r = 46.05$ m and 63.13 m ($U = 10$ m/s).

3. Results and Discussion

In order to assess the power-losses of the NREL 5MW wind turbine with contaminated blades, a numerical study that comprises typical operating conditions, contaminant particle sizes and heights is undertaken using the solution method outlined. Table 2 summarizes the wind speeds selected for the analyses and the corresponding operating conditions. The wind speeds selected encompass typical operating wind speeds of the turbine, including those below and above the rated wind speed, $U = 11$ m/s. Two contaminant particle sizes are studied, 40 and 150 microns. The first represents small contaminant particles, those that follow trajectories following streamlines and the second represents larger contaminant particles, those that follow ballistic trajectories. Two contaminant heights (also the roughness heights) are studied, i.e. $k_{s,max} = 0.2$ mm and 1 mm in order to bring out the effect of this parameter on the power-loss levels. The results are summarized in Figure 7.

It can be seen in Figure 7a and 7b that increasing roughness heights significantly reduce the power production. It can also be seen that small contaminant and roughness heights ($\sim$ 0.1-0.2 mm) have marginal effect on the production levels of the wind turbine. However, when the thickness reaches 1 mm, the effect is substantial. It can also be seen that, below the rated speed of the turbine, the power-losses are less significant, but quickly reach 14.2% and 16.7% for 40 and 150 micron contaminant particles, respectively, for a wind speed of $U = 14$ m/s. As the wind speed increases further, contamination casued by smaller particles results power-losses almost independent of wind speed. On the other hand, contamination caused by larger particles increasingly degrade the wind-turbine performance. As explained above, larger particles result in wider contaminated zones with higher contamination thicknesses that are distributed over a wider zone on the blade and hence they degrade the turbine performance more severely.

4. Conclusions

Power-losses due to blade contamination are calculated for a range of realistic operating conditions for the NREL 5MW wind turbine, combining well-known and proven computational methods in an in-house computational tool. The accuracy of the results can be improved by using a boundary-layer solution approach that takes flow separation into account. This is believed to represent the flow physics more faithfully, especially for conditions involving increased roughness and contamination thicknesses, where flow separation is likely. However, the present tool offers

a fast prediction method, which may be satisfactory for most practical purposes. The structure of the code also allows extensions to handle different phenomena, like erosion.

Table 2: Operating conditions used in the computations.

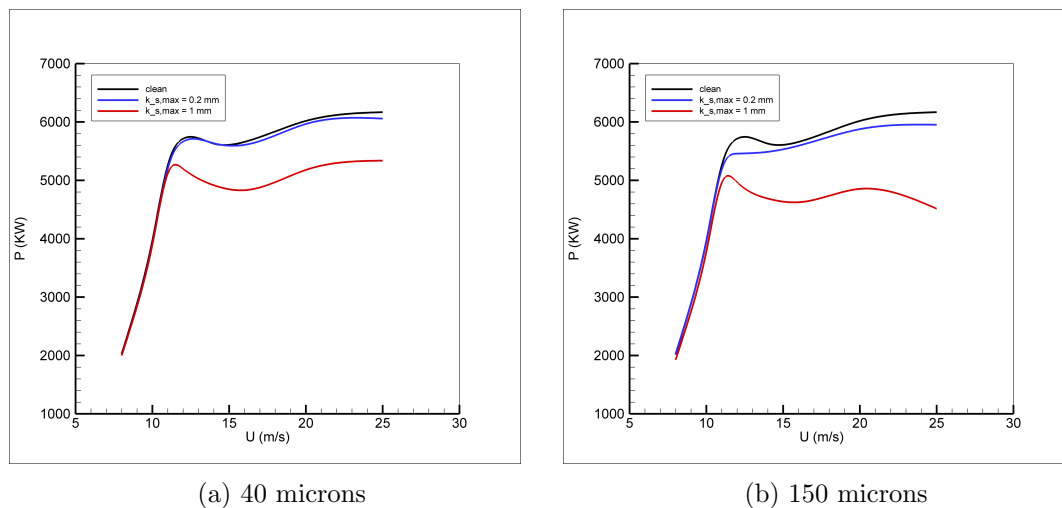| Wind speed, U (m/s)	Rotor rpm, Ω	Blade pitch (deg)	Tip speed ratio, λ_r
8	9.156	0.000	7.543
9	10.296	0.000	7.540
10	11.431	0.000	7.535
11	11.890	0.000	7.125
12	12.100	3.823	6.646
14	12.100	8.668	5.697
16	12.100	12.055	4.984
20	12.100	17.473	3.988
25	12.100	23.469	3.190

(a) 40 microns

(b) 150 microns

Figure 7: Power output with contaminated turbine blades.

References

[1] Han W, Kim J and Kim B 2018 *Renewable Energy* **115** 817–823
[2] Wilcox B and White E 2016 *Wind Energy* **19** 483–495
[3] Özgen S and Canıbek M 2009 *Heat Mass Transfer* **45** 305–322
[4] Özgen S and Canıbek M 2012 *The Aeronautical Journal* **116** 337–362
[5] Uğur N, Özgen S, Görgülü I and Tatar V 2017 *7th European Conference for Aeronautics and Space Sciences (EUCASS 2017)*
[6] Özgen S, Akyıldız E, Berker, AM and Çakmak A 2019 *8th European Conference for Aeronautics and Space Sciences (EUCASS 2019)*
[7] Manwell, JF, McGowan, JG and Rogers, AL 2010 *Wing Energy Explained: Theory, Design and Application* (Wiley)
[8] Virk M, Homola, MC and Nicklason, PJ 2012 *Int. J. Energy and Environment* **3** 1–8
[9] Katz J and Plotkin A 2001 *Low-Speed Aerodynamics* (Cambridge University Press)
[10] Gent, RW, Dart, NP and Cansdale, JT 2000 *Phil. Trans. R. Soc. Lond. A)* **358** 2873–2911
[11] White, FM 2006 *Viscous Fluid Flow* (McGraw-Hill)
[12] Schlichting, H 1979 *Boundary-Layer Theory* (McGraw-Hill)
[13] Kays, WM and Crawford, ME 1993 *Convective Heat and Mass Transfer* (McGraw-Hill)